

New benzene absorption cross sections in the VUV, relevance for Titan's upper atmosphere



Fernando J. Capalbo^{a,*}, Yves Bénilan^a, Nicolas Fray^a, Martin Schwell^a, Norbert Champion^{b,c}, Et-touhami Es-sebbar^a, Tommi T. Koskinen^d, Ivan Lehocki^a, Roger V. Yelle^d

^a Laboratoire Interuniversitaire des Systèmes Atmosphériques (LISA), UMR CNRS 7583, University Paris-Est Créteil (UPEC) and University Paris Diderot (UPD), 61 avenue du Général de Gaulle, 94010 Créteil, France

^b LERMA, Observatoire de Paris, PSL Research University, CNRS, UMR 8112, F-92190 Meudon, France

^c Sorbonne Universités, UPMC Univ. Paris 6, UMR 8112, LERMA, F-75005 Paris, France

^d Lunar and Planetary Laboratory, University of Arizona, Tucson, AZ 85721, USA

ARTICLE INFO

Article history:

Received 12 May 2015

Revised 1 September 2015

Accepted 6 October 2015

Available online 23 October 2015

Keywords:

Spectroscopy

Ultraviolet observations

Titan, atmosphere

Occultations

Atmospheres, composition

ABSTRACT

Benzene is an important molecule in Titan's atmosphere because it is a potential link between the gas phase and the organic solid phase. We measured photoabsorption in the ultraviolet by benzene gas at temperatures covering the range from room temperature to 215 K. We derived benzene absorption cross sections and analyzed them in terms of the transitions observed. No significant variation with measurement temperature was observed. We discuss the implications of our measurements for the derivation of benzene abundance profiles in Titan's thermosphere, by the Cassini/Ultraviolet Imaging Spectrograph (UVIS). The use of absorption cross sections at low temperature is recommended to avoid small systematic uncertainties in the profiles. We used our measurements, together with absorption cross sections from other molecules, to analyze four stellar occultations by Titan, measured by UVIS during flybys T21, T41, T41_II, and T53. We derived and compared benzene abundance profiles in Titan's thermosphere between approximately 530 and 1000 km, for different dates and geographical locations. The comparisons of our benzene profiles with each other, and with profiles from models of the upper atmosphere, point to a complex behavior that is not explained by current photochemical models.

© 2015 Elsevier Inc. All rights reserved.

1. Introduction

Titan's atmosphere is a rich reservoir of complex organic molecules. The identification and characterization of these molecules have been pursued with theoretical modeling of the atmosphere, laboratory experiments reproducing atmospheric conditions, and observations of the atmosphere itself. Among the complex hydrocarbons obtained in the models, experiments, and observed, is C₆H₆. From all the possible isomers with this elemental formula, this work deals with the cyclic form, *c*-C₆H₆, called benzene. Apart from its detection in Titan (Coustenis et al., 2003), benzene was also detected in Jupiter, Saturn (Bézar et al., 2001) and in the CRL618 nebula from ISO data (Cernicharo et al., 2001). It is the simplest of the aromatic hydrocarbons: a group of hydrocarbons characterized by alternating double and single bonds between carbons. Benzene is a potential precursor to the formation of a whole host of heavier hydrocarbons, including polycyclic aromatic hydrocarbons

(PAHs) and polyphenyls (Delitsky and McKay, 2010). The condensation of these aromatic compounds may contribute to the formation of Titan's haze layers (Wilson et al., 2003; Wilson and Atreya, 2003; Lebonnois, 2005). As a consequence benzene is one of the most interesting molecules detectable in Titan's atmosphere. In the remainder of this section we review the observations and models of benzene chemistry on Titan, as well as provide an overview of the previous measurements of its Vacuum Ultraviolet (VUV) absorption cross section.

1.1. Benzene on Titan

After the detection of benzene among the products of laboratory experiments simulating Titan's atmospheric chemistry (see for example Sanchez et al., 1966; Raulin et al., 1982; Coll et al., 1999; Imanaka et al., 2010), chemical models started to include this molecule. For example, motivated by the detection of polyaromatic compounds in laboratory tholins and theoretical work based on PAHs formation from benzene, Lebonnois et al. (2002) included it in their model for Titan's atmosphere and suggested chemical

* Corresponding author.

E-mail address: fernando.capalbo@lisa.u-pec.fr (F.J. Capalbo).

pathways that can link this simple molecule and PAHs to macromolecules, precursors to aerosol particles. However, this aerosol formation pathway was negligible in their model compared to others pathways (polymers of acetylene, polymers of HCN). This might be due to underestimated reaction rates, or to the low quantities of benzene in their model, small compared to the measured abundances given in Coustenis et al. (2003), derived from Infrared Space Observatory (ISO) spectra. These measurements constituted the first identification of benzene in Titan's atmosphere, with a mole fraction of $(4 \pm 3) \times 10^{-10}$ in the stratosphere. The detection of benzene triggered more attempts to model its production, and the inclusion of PAHs in the models for aerosol formation, particularly because of their importance as intermediate link in the gas-aerosol path, and haze formation. Wilson et al. (2003) analyzed mechanisms for the formation of benzene based on recombination of the propargyl radical (C_3H_3) and compared their results with the ISO observations. They found that ion chemistry plays a significant role on the formation of benzene above 750 km. The modeled benzene profile was updated in subsequent works (Wilson and Atreya, 2003, 2004), providing a better fit to the ISO measurements. Lebonnois (2005) presented a sensitivity study of $c\text{-}C_6H_6$ and PAHs on both Titan and Jupiter. In this model benzene was mostly produced by recombination of the propargyl radicals (C_3H_3), the benzene abundance was higher than that predicted by Lebonnois et al. (2002), and the PAH pathway was comparable to the other pathways considered for aerosol formation. The revised model agreed with the ISO measurements, the only observational constraints available at that time.

After the Cassini arrival to Saturn in 2004, observations provided stronger constraints on the models. The presence of benzene in the stratosphere was confirmed by Coustenis et al. (2007) and Vinatier et al. (2007) using data from the Composite Infrared Spectrometer (CIRS). The first of these references is based on nadir observations, and does not provide vertical profiles of the detected species. It presented an analysis of data from a Titan northern winter period, in which benzene was found to increase in abundance from some 3×10^{-10} at the equator to a maximum abundance of $(3.5 \pm 2.5) \times 10^{-9}$ at 70°N . The first vertical profile in the stratosphere was provided by Vinatier et al. (2007). Limited to 80°N during northern winter, the abundance increases with altitude from 3×10^{-9} (at about 160 km) to 5×10^{-9} (at about 320 km), although with overlapping uncertainties. They also provided an upper limit for $c\text{-}C_6H_6$ abundance of 1.1×10^{-9} in the southern hemisphere. Higher in the atmosphere (>900 km) measurements with the Ion and Neutral Mass Spectrometer (INMS, Waite et al., 2005; Vuitton et al., 2006, 2007; Cui et al., 2009), from several Cassini flybys, resulted in benzene abundances some orders of magnitude larger than the models predicted. Unexpectedly high abundances of other complex hydrocarbons were also derived. In this way, Cassini observations added new information about the benzene abundances in the stratosphere, and provided new constraints to the interpretation of its profile in the upper thermosphere.

The new observations were readily applied to improve the photochemical models. In their analysis of INMS data, Vuitton et al. (2007) provided a $c\text{-}C_6H_6$ mole fraction in the thermosphere derived from measured abundance of protonated benzene. They found higher concentrations in the thermosphere than previous results, which they associated to a production mechanism in the higher layers. On the other hand, the predictions of Lavvas et al. (2008) are below INMS results. For Lavvas et al. (2008) the main production process for benzene in the upper atmosphere was the recombination of two C_3H_3 radicals. Their analysis did not include the full ion chemistry that Vuitton et al. (2008) found to be critical for explaining high benzene densities. Vuitton et al. (2008)

presented a detailed study on the formation and distribution of $c\text{-}C_6H_6$ on Titan, using an ion chemistry model and a neutral chemistry model to analyze the production mechanisms in the atmosphere. The results were validated by comparison with INMS measurements from 12 flybys in the upper atmosphere and with CIRS values for the stratosphere. Vuitton et al. (2008), like Vuitton et al. (2007), suggested a main source of benzene in the thermosphere, where it is created mainly by ion chemistry. These latter works significantly improved the understanding of ion chemistry in Titan's atmosphere, and were followed by subsequent studies. De La Haye et al. (2008) developed a 1D ion-neutral rotating model to account for diurnal variations of solar irradiation. In their model two main processes are responsible for benzene production: neutral chemistry of C_3H_3 below 700 km, and electron recombination of $C_6H_7^+$ above 700 km. This last production mechanism is dominant in the thermosphere, as in Vuitton et al. (2008). In line with most of the recent studies, Krasnopolsky (2009), in their photochemical model of coupled neutral and ion chemistry of Titan, also favored ion chemistry over neutral chemistry for the formation of PAH in the upper atmosphere. Therefore, the latest studies suggest that the neutral pathway dominates in the upper stratosphere and mesosphere, while the ion chemistry pathway is important in the thermosphere.

Despite the agreement on the formation of benzene and other heavy molecules in the upper atmosphere of Titan, the detailed chemistry of benzene and other heavy species, and their role in forming organic molecules and aerosols, is still poorly understood. The profiles from the photochemical models have a large associated uncertainty (Hebrard et al., 2007), and change dramatically as a function of the chemical reactions involved. New atmospheric observations can help to solve the problems in the models. But the observations from Cassini/CIRS that probe the lower atmosphere are limited to altitudes below 300 km, while Cassini/INMS measurements of benzene in the thermosphere are limited to altitudes above 950 km. This leaves an important gap in the mesosphere/thermosphere, which is the transition region between the neutral and ion pathways to the formation of benzene, and a site of accelerated aerosol growth. Fortunately, this region can be probed by stellar occultations measured in the Far Ultraviolet (FUV) channel of the Cassini/UVIS instrument during Titan flybys. Koskinen et al. (2011) presented the first identification of benzene in this region based on the UVIS data, and provided two preliminary density profiles for flybys T41 and T53. These results were obtained by using the first release of the $c\text{-}C_6H_6$ absorption cross sections, measured at room temperature, resulting from the laboratory measurements presented in Section 2. Here we present revised density profiles of benzene for the two occultations analyzed previously by Koskinen et al. (2011), this time with an updated, low temperature, set of absorption cross sections for benzene (Section 3). In addition, we include new density profiles of benzene for two more occultations from flybys T21 and T41. We note that the study of more occultations, corresponding to different spatial/temporal coordinates, would facilitate the assessment of the variability and trends in the density profiles. Unfortunately, many of the Titan stellar occultations suffer from severe pointing drifts. The four presented here are, to the best of our knowledge, all of the stable occultations that benzene could be retrieved from prior to 2014.

1.2. Introduction to benzene absorption cross sections in the VUV

To interpret atmospheric absorption measured from stellar occultations, one needs quantitative absorption spectra of the molecules of interest. The interpretation of the absorption spectrum of benzene has served as a benchmark for the development and testing of theoretical approaches to describe π -electron

systems for a long time. Numerous experimental and theoretical studies have been carried out, particularly in the VUV spectral region. In some cases, published studies give no comments about resolution, uncertainties or the temperature (we assume 298 K) associated to the experiments.

The first measurements of VUV absorption of benzene were reported by Price and Wood (1935), who identified for the first time Rydberg transitions in the short wavelength region of the 1000–2000 Å range that they studied. Price and Walsh (1947) investigated the long wavelength region and identified tentatively at least two electronic transitions in the 1600–2000 Å region. The first studies presenting absolute absorption cross sections as a function of wavelength were those by Pickett et al. (1951), who used a photographic method to determine absolute values of extinction coefficients measured in the range 1560–2200 Å. Hammond and Price (1955) used a photoelectric detector to determine absorption cross sections in the range 1650–2150 Å. From the plots in these last two cited studies, both resolutions are coarse compared to the present study (see Section 2). Koch and Otto (1972) used spectrally continuous synchrotron radiation from the DESY electron accelerator to measure benzene absorption cross sections in the photon energy range of 6–35 eV (350–2060 Å), with a wavelength resolution between 1 and 4 Å. In their work they noted assigned Rydberg states, vibrational structures, and reviewed the first ionization energy values available at that time. Pantos et al. (1978) measured benzene extinction coefficients at room temperature, from 1350 to 2700 Å, at several resolutions. The resolution of the spectrum showed in their work is 2.5 Å. Their extinction measurements, that have been widely used in the literature, have an uncertainty of 10%. These are just some of the studies representing the first steps in interpreting the VUV absorption of benzene.

Newer experimental and theoretical studies allowed to further investigate the absorption in the UV and review old interpretations (see for example Grubb et al., 1985; Suto et al., 1992). Feng et al. (2002) provided a summary of the available absolute photoabsorption cross sections of benzene at different energy ranges, as well as a thorough comparison with previous results. Many other studies were referred to by Rennie et al. (1998), who measured absolute photoabsorption, photoionization, and photodissociation cross-sections, and the photoionization quantum efficiency of benzene and hexadeuterobenzene, in the range 350–1300 Å. The resolution ranged from 1.7 to 2.3 Å in the range 1160–1340 Å.

In this work we present new measurements of the $c\text{-C}_6\text{H}_6$ absorption cross section in the region 1160–2200 Å, at a resolution of 1 Å, including its dependence on temperature (mainly in 1700–1900 Å). To our knowledge, this temperature dependence has not been reported previously. Our absorption measurements are described in Section 2, our results and their analysis in Section 3. We used our absorption cross sections for the detection of benzene in Titan with UVIS, using stellar occultations measured in its FUV range (1115–1900 Å). This technique and the UVIS data reduction are briefly described in Section 4. Benzene abundances in Titan's upper atmosphere are presented in Section 5. Finally, Section 6 provides overall conclusions.

2. Experimental measurements of benzene absorption cross section

The absorption cross sections were derived from absorption measurements of $c\text{-C}_6\text{H}_6$ gas contained in a cell, illuminated with VUV radiation. The requirements for the measurement of the VUV absorption cross sections spectrum of a molecular gas imposes technical specifications at different levels (source, gas handling, detectors, etc.). The use of a spectrally continuous,

temporally stable source is an advantage, as all the wavelengths in the continuum can be used, and the observed variations in intensity are independent of the source. Moreover, the Beer–Lambert law used to determine the absorption cross section assumes that the radiation used is monochromatic. In practice, however, any spectrometer provides a wavelength bandwidth. It is therefore desired that the instrumental bandwidth (or resolution) be smaller than the width of the features in the absorption cross section spectrum. Benzene presents wide absorption bands, the study of which can be done with moderate resolution (a few Angstroms). However, it also presents sharp Rydberg bands for which sub-Angstrom—more difficult to obtain—resolutions are needed (Pantos et al., 1978). Fortunately, the detection of benzene in the UVIS spectra depends mainly on large absorption bands, and to a lesser extent in the superimposed Rydberg transitions (Koskinen et al., 2011), allowing the use of moderate-resolution absorption cross sections to retrieve benzene from UVIS measurements. Apart from these spectroscopic constraints, VUV measurements impose the use of windowless gas chambers, or the use of windows transparent to ultraviolet radiation, as well as detectors operating in this wavelength range. Finally, as in any experiment as those presented here, temperature and pressure should be permanently monitored and controlled.

We addressed these experimental challenges with two experimental setups, selected based on technical and availability reasons. We used the synchrotron facility BESSY II, Berlin-Adlershof, Germany, to measure absorption in the wavelength range 1150–2200 Å, and to explore the effects of measurement temperature at short wavelengths and at long wavelengths. We then expanded our set of measurements with the 10 m VUV spectrograph at the Paris Observatory, Meudon, France, where we studied the effects of temperature in the region 1710–1910 Å. Each facility has its advantages and disadvantages. Synchrotron radiation is less wavelength-dependent and more collimated than the deuterium lamp used in Meudon. The measurement interface at BESSY II is user-oriented and the wavelength scale is provided by the beamline monochromator. At the same time, the higher the resolution the more time the measurements take, beam time can be scarce and the measurement campaign very resource consuming. With the setup in Meudon, on the other hand, the registration of a reference spectrum together with the benzene spectrum allowed a more accurate wavelength calibration. Better availability of the facility allowed more time for experiment preparation and for measurement. However, in this experiment the sample is illuminated with the full spectrum of the lamp at the same time, and photochemistry is important. This requires extra experimental efforts and reduces measurement time and resolution. The degradation with handling of the sensitive screens used as detectors is another limiting factor.

Some of the characteristics are common to the two experiments. The sample used was the product 109646 from Merck, reference substance for gas chromatography with a stated purity of better than 99.9%. No impurities were detected in any of the measurements performed. The volume of the cylindrical cell used for the measurements was about 950 cm³. The entrance and exit of the cell were sealed by LiF (MgF₂) for the measurements in Meudon) and MgF₂ windows, respectively. This allowed measurements down to the MgF₂ cutoff wavelength (about 1140 Å). The cell pressure was measured using 2 capacitance sensor gauges (MKS 127AA): one measured absolute pressure in the range up to 1 mbar, the other in the range up to 1000 mbar. The static pressure increased a few μbar (~1 μbar for measurements in Meudon) during the measurements due to air leaks, but this had a negligible effect on the experiments. The temperature inside the cell was measured with two type-K thermocouples fixed on the inside wall of the cell, and located at the opposite flat plates of the cylinder.

The different setups and procedures are described in the next subsections. More detailed information can be found in Capalbo (2014).

2.1. Absorption measurements with Synchrotron radiation, BESSY II facility

Synchrotron radiation (SR) from an electron storage ring is a spectrally continuous and well collimated light source for spectroscopy. It can be used in different wavelength ranges, including VUV. The experimental setup and schematics have been described by Ferradaz et al. (2009). The sample gas was irradiated with SR from the BESSY II storage ring using the 3-m normal incidence monochromator (NIM) dipole beamline. Measurements were performed in the 1150–2200 Å range, at 1 Å resolution and 3 points per resolution interval. The choice of these values was a compromise between resolution and measurement time. The wavelength values have a varying precision depending on the wavelength region studied, being of 0.17 Å in the worst case. The absolute accuracy of the monochromator was found to be of about 3 Å at this beamline. The SR spectra were solid shifted with respect to the spectra measured in Meudon (see below), the latter being calibrated using the Schumann–Runge dioxygen absorption bands. High energy stray light from the source was minimized by refocalization and strong collimation of the monochromatized beam. The effective optical path was 14.15 cm. The intensity of the beam at the exit of the cell was measured with an Electron Tubes Ltd 9402B solar blind photomultiplier (PM). A cold-cathode pressure gauge was used to check the stability of the empty cell base pressure ($\sim 10^{-2}$ μbar). The range of $c\text{-C}_6\text{H}_6$ pressure used was 6–375 μbar, much lower than the saturation pressure at the temperatures used (e.g. ~ 1000 μbar at 230 K). The temperature was controlled during the low temperature part of the experiment using a liquid nitrogen flow through the jacket that surrounds the cell. This flow was regulated by a cryogenic valve to keep the system at a desired temperature. The temperature variation during a measurement was about ± 2 K, due to liquid nitrogen injection cycles. The temperature gradient across the cell was about 15 K. The values given for low temperature measurements correspond to an average value.

A measurement series to obtain one $c\text{-C}_6\text{H}_6$ absorption cross section spectrum at a particular temperature, wavelength range, and pressure, consisted in an empty cell spectrum, followed by a sample spectrum, and finally a second empty cell spectrum. Several series were measured varying only the benzene pressure, to confirm repeatability and pressure independence of the results. During the measurements, the ring current in the storage ring, and consequently the intensity of the radiation beam, diminished with time between electron injections. Taking this into account, a vacuum spectrum was estimated, interpolating between the two recorded

vacuum spectra. From 26 absorption spectra, those measured at the same temperature were averaged in the wavelength regions where they overlapped, resulting in the spectra listed in Table 2.

2.2. Absorption measurements with a deuterium lamp source, Paris Observatory facility

The set up for this experiment is shown in Fig. 1. Radiation from a Heraeus D200 VUV deuterium (^2H) lamp was used as a continuum source. This presented a flux variation of about 0.1%/min, limiting exposure time. The non-collimated radiation entered directly the sample chamber through its few-centimeter aperture. This means the molecules were irradiated with a VUV radiation flux from 1140 to 4000 Å modulated in intensity according to the relative radiance spectrum of the lamp, and the transmission of the windows. This motivated the presence of a shutter valve between the source and the absorption cell to minimize photochemical degradation during sample injection. All measurements were performed in the 1710–1910 Å range, with a relative resolution ($\lambda/\Delta\lambda$) of 2000, and 7 points per resolution interval. The choice of these values was a compromise between resolution and exposure time of the detectors. The wavelength scale was calibrated using the Schumann–Runge dioxygen absorption bands (1750–1950 Å), measured with a resolving power of 50,000. The reference spectrum used is from Yoshino et al. (1992). A first-order calibration polynomial was used to wavelength-calibrate the benzene spectra. The accuracy of this procedure is of $(1\text{--}6) \times 10^{-2}$ Å. Given the configuration of the experiment, no stray light was expected from the environment. The optical path in this setup was 17.45 cm. After leaving the absorption cell, the beam entered the 10.7 m spectrograph through an interchangeable slit. The spectrum was recorded simultaneously on 2 FUJI photosensitive plates, with linear response in intensities over five orders of magnitude. More details about the instrument can be found in Capalbo (2014). It is worth noting the similarities between this instrument concept and the UVIS instrument in Cassini, the latter being, roughly, a reduced space version of the former. The empty cell base pressure was $\sim 10^{-1}$ μbar. The range of $c\text{-C}_6\text{H}_6$ pressure used was 5–15 μbar, much lower than the saturation pressure at the temperatures used (70 μbar at 210 K, Fray and Schmitt, 2009). A decrease in radiation intensity was observed due to photolytic solid deposits on the windows. This limited the exposure time and, therefore, resolution (as a wider slit was needed to satisfy S/N requirements). The windows of the lamp and cell were regularly cleaned to overcome this problem. A LAUDA Ultra-Kryomat RUL 80(-D) was in charge of keeping the system at a desired temperature. The temperature uncertainty was 1 K and the stability better than this.

A measurement series to obtain one $c\text{-C}_6\text{H}_6$ absorption cross section spectrum at a particular pressure and temperature was performed by recording subsequently an empty cell spectrum, a

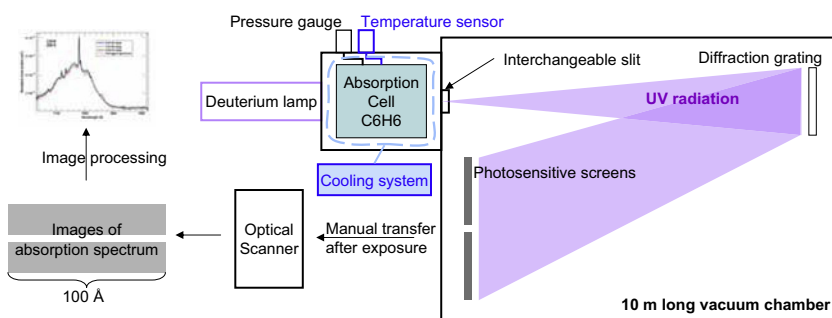


Fig. 1. Experimental setup used to measure benzene absorption cross section with a deuterium lamp as a source, at the Paris Observatory facility.

sample spectrum, and a second empty cell spectrum. Then a dioxygen spectrum was acquired for wavelength calibration purposes, measured at higher resolution. At least 3 different benzene pressures were explored for a given temperature, confirming repeatability and pressure independence of the results. As the source flux varied with time during the measurements, and assuming a linear decay in intensity, an average vacuum spectrum was calculated from the two vacuum spectra. The photosensitive image plates were then scanned to create a high resolution, 16-bit image in which the pixel values were proportional to the flux received by the screens. Tilts, image deformations, and image plate defects, which could produce unreal features in the spectra, were accounted for during processing. The rows in the images corresponding to exposed regions in the screens were averaged to get a spectrum (vacuum, benzene, or dioxygen). Unexposed regions in the plate were used to estimate a background correction. Spectra covering 200 Å were created from the two image plates, the gap between the plates (some 5 Å in the worst case) was filled with linearly interpolated values. From 12 absorption spectra, those measured at the same temperature were averaged, resulting in the spectra listed in Table 2.

2.3. Absorption cross section derivation and uncertainties

Transmission was determined from the ratio of the measured benzene spectra and vacuum spectra. From the transmission, the absorption cross section was calculated using the Beer–Lambert law in the form

$$T = \frac{I}{I_0} = \exp\left(-\tilde{\sigma}l\frac{p}{T}\frac{T_0}{p_0}\right), \quad (1)$$

where the transmission as a function of wavelength, T , is the ratio of the sample spectrum I to the vacuum spectrum I_0 . The absorption cross section is $\tilde{\sigma}$, in units of $\text{amagat}^{-1}\text{cm}^{-1}$. The optical path through the absorption cell is l ; p and T are the pressure and the temperature in the cell, respectively; $T_0 = 273.15\text{ K}$, and $p_0 = 1013.25 \times 10^3\text{ mbar}$. The absorption cross section presented in the following sections was calculated according to

$$\sigma = \tilde{\sigma}/n_0, \quad (2)$$

where σ is in units of cm^2 , and n_0 is the Loschmidt constant $2.6867805 \times 10^{19}\text{ cm}^{-3}$.

It is very difficult to obtain acceptable absorption measurements in a whole wavelength range where the absorption varies significantly. Low gas pressure in the absorption cell would allow clear measurements of strong absorption regions, but noisy measurements in regions of weak absorption, where the latter could not be clearly determined. High gas pressures in the cell would allow measurements of smaller absorption coefficients, but might saturate strong absorption features. In the range 1700–1900 Å

the benzene absorption cross section varies by a factor larger than 12. The region around maximum absorption was given priority in this work. As a result, the measurements from the Meudon experiment above 1840 Å are very noisy. Nevertheless, the whole measured range was kept to provide a comparative value with the measurements performed with the SR source.

There were random and systematic sources of uncertainty. Systematic uncertainties have an upper limit of $\sim 4.5\%$. These include uncertainties in the optical path (less than 0.5%), in the temperature (maximum of $\sim 4\%$), and in the measurement of pressure (maximum of $\sim 2\%$). Random uncertainties include uncertainties in the PM current, or in the digital values extracted from the sensitive screens (both less than 0.3%). Moreover, as the absorption cross section is independent of pressure (see above), several absorption cross section spectra determined from measurements obtained with equal experimental conditions, but different pressure, can be interpreted as different determinations of the same quantity, and serve to further characterize the random variations in our results. This is the most important source of uncertainty in the derived cross sections. Therefore, for a particular spectrum the random uncertainty was calculated as the relative difference between absorption cross sections measured at two extreme pressures (i.e. two extreme transmissions), and is given by

$$\delta\sigma_\lambda = \frac{\sigma_{\lambda,\text{plow}} - \sigma_{\lambda,\text{phigh}}}{\sigma_{\lambda,\text{plow}} + \sigma_{\lambda,\text{phigh}}}, \quad (3)$$

where *plow* and *phigh* represent the lowest pressure and highest pressure measured, respectively, in the wavelength range considered. This resulted in different uncertainty associated to different spectra and wavelength regions, according to different experimental conditions. For spectral regions where only one pressure was available, the uncertainty could be estimated from measurements in neighboring wavelength regions, and/or measurements at similar temperatures. Table 1 summarizes the random uncertainties corresponding to each spectrum presented, the limits of the wavelength regions indicated are approximate.

Finally, it is worth mentioning that the instrumental bandwidth was greater than the line width of the Rydberg transitions (see for example Pantos et al., 1978). Therefore, the absorption cross section values for the thinner peaks in the spectra might be in these cases underestimated due to this experimental constraint (see discussion in Section 3). The valence transitions measured, much broader, do not suffer from this problem.

3. Absorption cross section results and interpretation

The characteristics of the final spectra are presented in Table 2. Fig. 2 shows the absorption cross section measured at 298 K, covering the full wavelength range studied. The borders of the wavelength range of the FUV channel of the UVIS instrument, used

Table 1

Random uncertainties corresponding to each spectrum derived in this work, and presented in Table 2. The limits of the wavelength regions indicated are approximate.

Absorption cross section uncertainty (%) for measurements with deuterium lamp source				
Temperature (K)	Wavelength range (Å)			
	1710–1740	1740–1830	1830–1910	
295, 245, 215	10	5	20	
Absorption cross section uncertainty (%) for measurements with SR source				
Temperature (K)	Wavelength range (Å)			
	1150–1360	1360–1600	1600–1800	1800–2040
298	4	7	3	3
250	<14	<14	<14	
230			7	

Table 2

List of measured spectra. Spectra from the bibliography shown in Fig. 2 are also included for reference.

Reference	Temperature (K)	Range (Å)	Resolution (Å)
This work, SR	298	1203–2103	1
This work, ² H	295	1715–1910	1
This work, SR	250	1153–1600	1
This work, ² H	245	1715–1910	1
This work, SR	230	1723–1823	1
This work, ² H	215	1715–1910	1
Pickett et al. (1951)	298	1538–2119	<i>n</i> ^a
Hammond and Price (1955)	298	1613–2128	<i>n</i> ^a
Pantos et al. (1978)	293–300	1352–2108	2.5
Rennie et al. (1998)	298	348–1341	1.7–2.3

^a *n* = not specified.

to retrieve hydrocarbon density profiles, are shown as dashed lines. In the following we will identify some of the transitions in our measured spectrum and compare them with previous work, but our intention is not to provide a thorough interpretation of the benzene absorption bands—this has been done before. Nevertheless, our data provide new experimental material that can be used for that interpretation. Our focus is on the general absorption features in the measured spectrum, in the range relevant for the FUV channel of the UVIS instrument (1115–1900 Å), their variations with temperature, and their use to identify benzene in Titan's upper atmosphere.

As can be seen in Fig. 2, it is difficult to identify band system onsets in the spectrum, due to the overlapping of the neighboring systems and the presence of a continuum. In VUV spectroscopy of polyatomic molecules, valence shell transitions are mixed in with transitions to higher excited states, in which the excited electrons occupy diffuse Rydberg orbitals with large principal quantum numbers. Even at the moderate resolution of our measurements, however, some band systems and transitions can be identified. Benzene absorption in the wavelength region studied here is 3 orders of magnitude stronger than in the region around 2500 Å, where forbidden transitions are located (see for example Fally et al., 2009). This explains the steep decrease of the absorption cross section above 2050 Å. The absorption for wavelengths shorter than those shown here corresponds to other Rydberg states (see for example Rennie et al., 1998). The spectrum in Fig. 2 may be roughly divided into 4 regions. In the region 2050–1850 Å there is a system of diffuse bands. The absorption in the region from 2000 to 1800 Å was interpreted in two different ways (see Pickett et al., 1951; Herzberg, 1966 and references therein). It was believed by Carr and Stuecklen (1939) and Hammond et al. (1950) to constitute the first member of the second Rydberg series previously reported by Price and Wood (1935) and co-workers. It has also been associated with the forbidden transition $^1A_{1g} \rightarrow ^1B_{1u}$ (see for example Feng et al., 2002; Koch and Otto, 1972).

The second region, 1850–1600 Å, presents a strong, broad absorption with a few sharp peaks and an underlying continuum. It was believed by Pickett et al. (1951) to represent two transitions, a Rydberg series overlying a valence π -electron transition of type $^1A_{1g} \rightarrow ^1E_{1u}$ (Herzberg, 1966; Pantos et al., 1978)—this is the only symmetry-allowed transition in the D_{6h} point group (Hammond and Price, 1955). The peak at 1789.45 Å in our spectrum (1789.09 Å in Pantos et al. (1978), 1790 Å in Pickett et al. (1951), 1786.52 Å in Koch and Otto (1972)), and the accompanying sharp bands were suggested to represent the first member of the second Rydberg transition in Price and Wood (1935), converging to the first ionization energy (IE) of 9.24378 eV¹ (1341.27 Å).

The 'shoulders' with maxima around 1781 Å and 1804 Å in our spectra were confirmed by Koch and Otto (1972) to be part of the underlying valence transition.

The narrow bands in the region 1600–1350 Å get weaker and closer to each other towards shorter wavelengths, and merge into an absorption continuum at the IE. The sharp bands in this region have been assigned to Rydberg series with their corresponding vibrations (see for example Price and Wood, 1935; Herzberg, 1966; Pantos et al., 1978; Grubb et al., 1985). Some of the series converge to the first IE, others to the second IE at 11.45 eV (1083 Å).

The spectral features in the fourth region, covering 1355–1150 Å, are considerably more diffuse than those at wavelengths longer than 1360 Å. Koch and Otto (1972) identified, with the help of photoelectron spectra from Turner (1970), that the groups of bands seen in our spectra are the first ($n = 3$, the group close to 1350 Å) and second ($n = 4$, the group close to 1150 Å) members of a Rydberg series and associated vibrations, converging to the second IE. Other Rydberg series, also visible in our measurements, converges to the third IE, found at 11.71 eV (1060 Å Koch and Otto, 1976). This region has also been remeasured and interpreted with the aid of photoelectron spectra by Rennie et al. (1998).

Pantos et al. (1978) underlined the importance of the effect of the instrumental bandwidth. The Beer–Lambert law is correctly used to obtain the cross section only when the exciting light bandwidth is much less than the intrinsic line width of an absorption line. This is the case for the $^1A_{1g} \rightarrow ^1B_{1u}$ transition, for which they found no significant variation with bandwidth, and for the $^1A_{1g} \rightarrow ^1E_{1u}$ transition. But for the Rydberg bands our bandwidth was larger than the widths of the lines (line widths of ~ 0.1 Å should be expected in the Rydberg region according to Pantos et al., 1978). In these cases the derived absorption cross sections might be underestimated. This is not expected to affect the identification of benzene on Titan in the UVIS observations, because the identification is mostly based on the large feature associated to the $^1A_{1g} \rightarrow ^1E_{1u}$ valence transition. However, in our spectrum measured at 215 K (see Section 3.1), the peak at 1789.45 Å, associated to the first member of the second Rydberg series in Price and Wood (1935), is about 1.7 times bigger than the maximum of the valence transition. Thus, for the detection of benzene with a higher resolution than that of the UVIS instrument, the effect of this peak in the detection, as well as the dependence of the peak with bandwidth, should be further explored, and attention should be paid to the resolution of the absorption cross section used.

Fig. 2 shows results from four other studies (Pickett et al., 1951; Hammond and Price, 1955; Pantos et al., 1978; Rennie et al., 1998). Tabulated data from the first, second and fourth reference were downloaded² already in the units plotted here. Data from the third reference was read from their Fig. 3. For the first three references, extinction coefficients have been read from the original work and converted to absorption cross sections (conversion factor 3.8235×10^{-21}). The absorption cross section presented in Suto et al. (1992) and measured at 1 Å resolution (not shown here) agree with those from Pantos et al. (1978) within the 10% uncertainty in the newer results. Improved resolution in our work permits to identify vibrational features absent in the old spectra, particularly the bands around 1759 Å and 1767 Å. The best agreement in absolute value is with the data from Pantos et al. (1978). The ratios of the maximum value in our spectrum over the maxima in the spectra from the references are 0.76, 1.49, and 1.13, for the values from Pickett et al. (1951), Hammond and Price (1955), and Pantos et al. (1978), respectively. The relative difference between our maximum and those in the references are in all cases bigger than the 5% total

¹ NIST Chemistry WebBook. <http://webbook.nist.gov/cgi/cbook.cgi?ID=C71432&Units=SI&Mask=20#Ion-Energetics>, January 2015.

² Downloaded from <http://www.atmosphere.mpg.de/>, 2014.

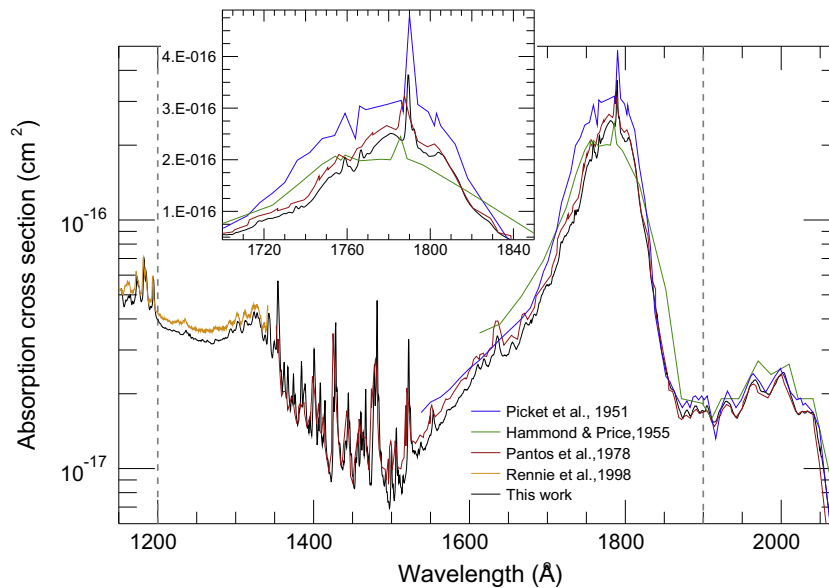


Fig. 2. Benzene absorption cross section measured with SR as a source, at 298 K. Measurements from other work are shown for comparison. The inset shows the most relevant region for benzene detection in Titan, with the UVIS instrument. The wavelength range of the FUV channel of the UVIS instrument, used to retrieve hydrocarbon density profiles, is shown as dashed lines.

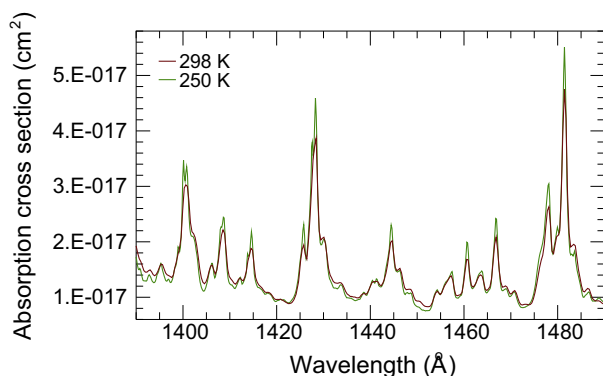


Fig. 3. Benzene absorption cross section measured at two different temperatures, 298 K and 250 K, in the range 1390–1490 Å.

uncertainty in our measurements. There are small shifts in wavelength between our spectrum and those in the references, probably due to the reading process or the higher resolution in our data. A more detailed comparison of the spectra is out of the scope of the present work. Nevertheless, it is clear that our measurements make a significant contribution for the interpretation and applications of the absorption spectrum of benzene.

3.1. Temperature variations

One of the main motivations of this work was to study the response of the benzene absorption cross section to temperature variations. From the pure spectroscopic point of view, even at the moderate resolution of our measurements, it is useful to see the reaction of the different band systems when lowering the temperature. Besides, the knowledge about the variation of the absorption cross section with temperature is of primary importance for atmospheric VUV spectroscopy. In our particular case, the interest focuses on absorption cross sections measured at temperatures rel-

evant to the upper atmosphere of Titan (~ 150 K, see Cui et al., 2009; Snowden et al., 2013), or in the confirmation of the absence of significant variations with temperature, at least at the resolution of UVIS. Pickett et al. (1951) mentioned that the relative intensity of the first two bands in the 2000 Å region (reading the spectrum from the long wavelength end), measured at 253 K, showed no measurable change with respect to the measurements at room temperature. Apart from this comment, we found no systematic study of temperature variations of the benzene absorption cross section in the VUV region studied here. For these reasons we measured absorption at different temperatures, and analyzed the variation in the absorption cross sections as a function of temperature.

Fig. 3 shows spectra at two different temperatures (298 and 250 K) for the range 1390–1490 Å. The figure shows that some bands get narrower and increase in height when the temperature decreases, while other local maxima decrease. This behavior was expected, since collision rates decrease and lower ro-vibronic levels get more populated when the temperature decreases. Some bands representing weaker transitions, at the sides of a stronger one, decrease with decreasing temperature. These correspond to transitions from higher vibrational energy levels, whose population decreases with decreasing temperature, and consequently the intensity of the associated absorption. Although some of the variations observed correspond to real changes with temperature, variations of the position of the maxima in wavelength which are smaller than the 0.17 Å measurement precision (see Section 2.1) should not be taken into account.

Spectra at different temperatures for the range 1700–2050 Å are shown in Fig. 4. The difference in the region 1715–1820 Å, between the measurements performed at room temperature with the two different instruments described in Section 2, is less than 10% (less than 5% for most of the wavelength range). This is an indication of the reproducibility of the measurements. Indeed, both spectra were measured at almost the same temperature, with the two different experimental setups presented; the fact that the residual is within the limits of the uncertainty in the measurements verifies the coherence of the results, and validates further comparison of results derived from the different experiments.

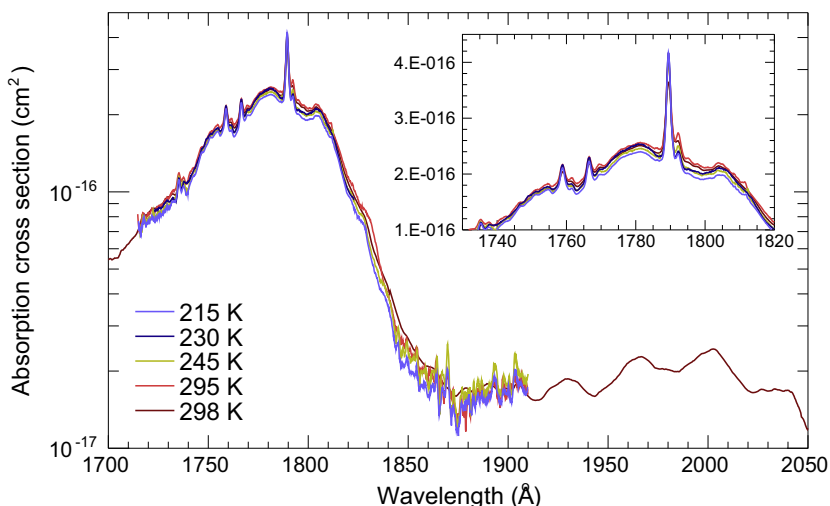


Fig. 4. Benzene absorption cross section at different temperatures, in the range 1700–2050 Å.

The curves for 245 K, 230 K, and 215 K in Fig. 4 present a common overall behavior. The absorption cross section decreases with decreasing temperature in most of the wavelength range 1730–1820 Å (shown in the inset of Fig. 4). The biggest decrease is observed for wavelengths at the local minima in the absorption cross section. For some of the local maxima the behavior is opposite, the absorption increasing with decreasing temperature, while the width of the associated bands diminishes. This is evident for the local maxima around 1760 Å (only for the 230 K curve) and for the global maximum in the region, close to 1790 Å. These variations with temperature are consistent with the explanations in terms of population of levels given above. Even though most of the observed variations with temperature remain within the measurement uncertainty (see Table 2), some significant variations (greater than the uncertainty) as a function of temperature are observed. These include the variation of the maximum close to 1790 Å. Other significant variations are seen for some of the minima, particularly, the minimum around 1791.5 Å. These variations in the minima are more evident for the curve corresponding to measurements at 215 K.

The identification of benzene in the UVIS spectrum is based on the ${}^1A_{1g} \rightarrow {}^1E_{1u}$ intense absorption, and to lesser extent on the over-imposed Rydberg peaks. Significant variations with temperature, of up to 10% (14% in the Rydberg maximum), are observed within this spectral range. The relative uncertainty in the transmission measured by UVIS in this region, for altitudes of 650 km and 800 km, is around 6–15%. Therefore, non trivial effects on the retrieval of benzene on Titan with UVIS due to variations of the absorption cross section with temperature could, in principle, be expected (we show in Section 5, however, that the effects are within the uncertainty in the number density), and the absorption cross section measured at 215 K should be used. On the other hand, 215 K is the lowest temperature explored here, while Titan's atmosphere can be as cold as ~ 120 K (see for example Snowden et al., 2013). However, going from 215 to 120 K, the population of the vibrational ground state increases by $\sim 18\%$. The corresponding change between 298 K and 215 K is $\sim 26\%$, and the variation in absorption cross section about 10%, as commented above. The change in the absorption cross section between 215 K and 120 K is then expected to be less than 8%. Therefore, an influence on the $c\text{-C}_6\text{H}_6$ retrieval from UVIS data, caused by a temperature effect on the absorption cross section is not expected in this case, and the use of absorption cross sections measured at 215 K is justifiable for the analysis.

4. Analysis of stellar occultations observed by UVIS

This section briefly describes the data and methods used to derive atmospheric composition. This was done by combining absorption cross sections from laboratory measurements, and stellar occultations measured with the far ultraviolet (FUV: 1115–1913 Å) channel of the UVIS instrument, aboard the Cassini spacecraft. For a more detailed description of the instrument and its data see Esposito et al. (2004). More information and details about the occultation technique, VUV occultations, data, and data reduction (including geometrical calculations and the retrieval procedure) can be found in Koskinen et al. (2011), LASP (2014), Capalbo (2014), and references therein.

4.1. Atmospheric composition from absorptive VUV stellar occultations

During occultations the spectrum of the star is observed along different lines of sight through the atmosphere. These spectra are divided by the unattenuated spectrum observed outside of the atmosphere, to obtain transmission. The measured transmission is determined by the absorption of the different species at different altitudes. Absorption is the dominant phenomena for the observations analyzed here, although extinction from aerosols is also considered. Ultraviolet airglow from Titan's atmosphere (Ajello et al., 2007, 2008), scattered radiation into the instrument FOV, and refraction effects can be neglected (Koskinen et al., 2011).

This work focuses on benzene. The other molecules considered to perform the retrieval of abundances are methane (CH_4), acetylene (C_2H_2), hydrogen cyanide (HCN), ethylene (C_2H_4), diacetylene (C_4H_2), cyanoacetylene (HC_3N), and aerosols (AER). These have already been identified in the FUV spectrum of Titan (Shemansky et al., 2005; Koskinen et al., 2011). Our choice of molecules was also founded on an analysis of theoretical detectability of different species based on their absorption cross section, their model-predicted abundances in the atmosphere, as well as UVIS resolution and S/N (Capalbo, 2014). The absorption cross sections of the molecular species (other than benzene, see Section 3) and the extinction cross sections of aerosols, used in the retrieval of atmospheric constituents, can be found in Koskinen et al. (2011) and in Capalbo (2014). The molecular absorption cross sections were measured in laboratory, the extinction cross sections for the aerosols were calculated for spherical aerosols with a radius of 100 Å, using Mie theory and assuming the optical properties of

tholins (Khare et al., 1984; Koskinen et al., 2011). This choice is irrelevant to the task of separating aerosols from the other absorbers.

For each tangent altitude (i.e., the shortest distance from the line of sight to the surface of Titan), the column densities were determined from comparisons of modeled transmission with measured transmission. The column densities were inverted to obtain number density profiles. These inversion problems are generally ill-posed. So, the column density profiles were retrieved using a χ^2 -minimization technique, and the number density profiles were retrieved using a constrained linear inversion method. Very similar procedures have been used before to analyze occultations (Vervack et al., 2004; Quemerais et al., 2006; Koskinen et al., 2011) and the technique presented here follows them closely. A detailed step by step explanation of the procedure is given in Capalbo (2014), while a summary of the procedure follows.

4.1.1. Column density retrieval

In order to separate different absorbers, and to retrieve their column densities, we fitted the transmission spectra at each tangent altitude. The model used to fit the data involved the absorption cross sections of the species considered and a convolution with the instrument response, that we modeled as a Gaussian with a 2.38 Å width and two Lorentzians, one of width 34.44 Å, the other of width 392.35 Å (see the UVIS User's guide, LASP, 2014). In the general case, the absorption cross sections (or extinction cross section for the aerosols) depend on temperature, and consequently on altitude. In this work the absorption cross sections were considered independent of altitude, and absorption cross sections measured at low temperatures were used when available. The optimal column densities were determined by using the Levenberg–Marquardt (see for example Press et al., 1996) minimization algorithm with the IDL routine MPFIT (Markwardt, 2009), wrapped in an iteration scheme to work around unphysical values that can result from the non-convergence of the routine to a minimum.

To exclude meaningless results in the extremes of the altitude range (due to transmission values very close to one or to zero), the column density profiles were restricted in altitude. The valid altitudes in the profile of a particular species were defined as those for which the transmission was roughly between 0.01 and 0.99, for wavelength regions where the species has characteristic absorption. Outliers and abundances for which MPFIT could not provide a value and a consistent uncertainty, were replaced by interpolated values, assuming a decreasing exponential behavior as a function of altitude. Interpolated values in the final column density profiles remain rare: only 1–10 altitudes, normally in the lower or upper boundaries of the profiles, and mainly for HCN, HC₃N, c-C₆H₆, and AER. No values were extrapolated.

4.1.2. Number density and aerosol extinction retrieval

The number densities were determined by using a constrained inversion of the column density profiles, or Tikhonov regularization (see for example Quemerais et al., 2006). The constraint was based on the assumption of smoothness of the solution, and implemented via a second derivative operator. The intensity of the regularization is given by the regularization parameter λ . The determination of λ is key in the process, and several criteria are possible. A small value of λ would result in a noisy profile. If λ is too big, too much smoothing will produce a featureless profile. The details of our implementation of the Tikhonov algorithm are in Capalbo (2014). The resolution of the retrieved profiles are determined by the so-called averaging kernel matrix.

Some of the values in the retrieved profile are not shown because the inversion failed to provide a reasonable value and

uncertainty. These values are in most cases in the minima, or the lower altitudes of the number density profiles. Moreover, values within one resolution width from the top of the profiles were eliminated, to account for a border effect due to the second derivative operator used in the inversion. The different points in the profile have similar but different altitude resolutions. The median of the resolutions is reported as a characteristic resolution for the whole profile. The routines developed to retrieve the number densities from the measured transmission were validated with simulated data as described in Capalbo (2014).

4.1.3. Uncertainties and benzene identification

There are several sources of uncertainties associated with the analysis. The uncertainty coming from the Poisson counting statistics in the detector is propagated in the calculation of transmission and optical depth. The MPFIT routine provides the 1- σ uncertainties of the column densities, determined from the spectral fit. The uncertainties in the number densities are evaluated by means of a formal error propagation through the inversion routine. The systematic uncertainty coming from the measured absorption cross sections (up to 10% in the worst cases), are not included in the final uncertainties. Our analysis based on simulated data shows that the uncertainties from MPFIT are often underestimated. However, the analysis showed that, for most of the altitudes, the 'true' number density profiles were retrieved to within 2 σ . Thus, we recommend the 2- σ uncertainty interval to be used when interpreting the results in Section 5.

The retrieval techniques used to derive the density profiles of the species are based on their absorption cross section. But the technique itself is unable to identify a molecule given an absorption cross section spectrum, the identity of the molecule is determined by the 'user'. This is based not only on the confidence that the absorption cross section used corresponds to the molecule of interest, but also on the confidence on the correlation of features in both the absorption cross section and the measured spectrum. The question might then arise about the true identity of a particular species, particularly when isotopic substitution, or substituted molecules (like substituted benzenes), can lead to absorption spectra similar to that of the molecule of interest. The sets of absorption bands obtained in both light benzene and heavy benzene are essentially similar (Price and Wood, 1935; Rennie et al., 1998). However, those of the latter suffer a small shift to the violet relative to those of the former. Moreover, the *D/H* ratio measured for Titan by different techniques is about 10⁻⁴ (Table 10.4 in Soderblom et al., 2009). Other benzene derivatives present absorption cross sections similar to those of benzene (see for example Hammond et al., 1950; Suto et al., 1992). But the main valence transition, and the over-imposed Rydberg transition around 1790 Å in the benzene absorption cross section (see Section 3), that actually determine its presence in the UVIS FUV spectrum, are shifted in the benzene derivatives by more than the UVIS spectral resolution (except maybe for benzotrifluoride, which is irrelevant for studies of Titan's atmospheric chemistry). Moreover, the abundance of more complex aromatic rings is expected to be lower than that of benzene and, thus, also their contribution to absorption. All this strongly suggests that the species we retrieved using the absorption cross section presented in this work is, indeed, benzene.

4.2. UVIS observations analyzed

Geometric and other ancillary information about the stellar occultations analyzed in this work is presented in Table 3. The geometry of observation was calculated with the help of the SPICE information system and the SPICE toolkit, from the Navigation and Ancillary Information Facility (NAIF, Acton, 1996). The integration

Table 3
Characteristics of the stellar occultations analyzed.

Flyby	Data product (FUV/yyyy_doy_hh_mm)	Star	Lat. (deg) ^a	Lon. (deg W) ^a	Atmosp. in shadow ^a	Altitudes probed (km)	Original sampling (km) ^a	S/c – TA min. ^b (km) ^a
T21	FUV2006_346_10_39	α Eri	–35 to –36	116–119	No	0–2330	3.8	1.6×10^4
T41	FUV2008_054_15_36	ϵ CMa	–2 to –10	332–334	Yes	243–2000	0.4	4.7×10^5
T41_II	FUV2008_054_21_31	ϵ CMa	–24 to –28	173–175	No	72–3044	0.8	6.0×10^5
T53	FUV2009_109_21_23	α Eri	38–39	294–308	No	0–4627	1.6	3.8×10^4

^a For altitudes relevant to absorption measurements.

^b Spacecraft – tangent altitude minimum distance.

duration for each spectrum, the spacecraft velocity, and the spacecraft attitude determined the vertical sampling of the atmosphere. The integration time was 1.75 s for the stellar occultations analyzed here; the sampling of the atmosphere varied slightly from one occultation to the other, between 0.5 and 4 km. The altitude sampling was, after altitude averaging to improve *S/N*, around 10 km. The final vertical resolution was determined by the number density retrieval process (see Section 4.1). Although the reflection of light by the atmosphere and UV airglow are negligible for a 1–2 s exposure, solar illumination can affect the chemistry and composition of the atmosphere (see for example De La Haye et al., 2008). It is therefore useful to know if the atmosphere probed by the occultation was in shadow or not. This information is given in the sixth column of Table 3.

During the data reduction process, the dark current of the instrument and the background (determined from the counts measured low in the atmosphere, where no photons from the source are expected to reach the detector) were negligible. The effect of low response (‘evil’) pixels in the detector was corrected by linear wavelength-interpolation (see UVIS User’s Guide, LASP, 2014). For the occultation data products analyzed in this work, 5 rows in the detector correspond to useful data, the corresponding rows were summed up. The result is a 2-D matrix containing count values for wavelength–time (or tangent altitude) coordinates.

Four occultations were analyzed in this work: T21, T41, T41_II, and T53. These were chosen because of their pointing stability, and because our results from T41 and T53 can be compared with those derived previously for these flybys (Koskinen et al., 2011), with an almost identical technique. The profiles derived cover altitudes roughly from 350 to 1200 km, which lie in between of those covered by CIRS and INMS. In general, the span in longitude and latitude for the relevant altitudes is only a few degrees. Hence, the profiles derived from UVIS data can be considered as real vertical profiles. The star occulted during flybys T21 and T53 was Alpha Eridani (Achernar), the star occulted during flybys T41 and T41_II was Epsilon Canis Majoris (Adara).

5. Titan’s atmospheric composition

5.1. Previous results from UVIS FUV stellar occultation s

Stellar UVIS FUV occultations by Titan were first presented by Shemansky et al. (2005). From the occultations measured during flyby Tb, they derived column density profiles for CH₄, C₂H₂, HCN, C₂H₄, C₂H₆, and C₄H₂. The observations covered altitudes from 450 to 1600 km above the surface. The C₄H₂ absorption cross sections used by Shemansky et al. (2005) were saturated at 1445 Å and 1645 Å, which might have led to an overestimation of the abundance for this species. Liang et al. (2007) used the same UVIS data from the Tb flyby to detect and characterize aerosols, at altitudes between 500 and 1000 km. The detection of aerosols in this region implies that they are formed at higher altitudes in the ther-

mosphere. The results of Koskinen et al. (2011), based on occultations T41 and T53, significantly expanded on the previous analysis of UVIS FUV occultations. They led to the identification of new absorbers in the data (C₆H₆ and HC₃N), the detection and characterization of aerosol layers in the upper atmosphere, the retrieval of detailed density profiles for 7 gaseous species, and the detection of large scale waves in Titan’s mesosphere. Capalbo (2014) included a thorough analysis and characterization of the retrieval techniques to derive composition from UVIS FUV stellar occultations. In the present work, the technique was applied to data from flybys T21, T41, T41_II, and T53. We present new *c*-C₆H₆ profiles, obtained for the first time with the absorption cross sections measured at low temperature (see Section 3). We note that the density profiles are obtained simultaneously for all 8 absorbers, but here we limit our focus to benzene.

5.2. Column densities and residuals

We obtained column density profiles for all the species included in the model, and for the 4 occultations. As the minimum of the cost function depends on the line of sight abundance of all the species, none of them can be assessed independently, and the output of the spectral fit as a whole has to be taken into account. The quality of the column densities obtained can be estimated from the value of the reduced χ^2 (χ^2_R) and the residuals between the model and the observations. The χ^2_R is the value of the χ^2 quantity divided by the degrees of freedom (number of wavelength bands contributing to χ^2 minus the number of parameters). The χ^2_R fell for most of the altitudes in the range 0.85–1.45 for T21, the ranges were 0.7–2.6 for T41, 1.0–2.0 for T41_II, and 0.8–1.8 in the case of T53. These values imply a good fit. The normalized residuals are the difference between the modeled transmission (computed from the retrieved column densities) and the measured transmission, divided by the uncertainty in the measured transmission. Examples of the measured transmission and the modeled transmission at 500 km, 800 km, and 1000 km, from flybys T21 and T41_II, are shown in Fig. 5. The corresponding residuals are shown in Fig. 6. As the quality of the fit varies with altitude, a species in the model could be missing or underestimated (positive residual), or overestimated (negative residual), for some altitudes. A thorough analysis of the transmission and the residuals is out of the scope of the present work. However, some characteristics are worth mentioning. According to the tests of performance of the retrieval technique, only residuals larger than 2σ are significant. Isolated peaks, at individual wavelengths, are not interpreted as coming from an absorbing species. Below 600 km the transmission below ~ 1500 Å (and for some individual values around 1630 Å and 1700 Å in the case of T21) is practically zero, and the calculated residual has no physical significance. The same happens below 800 km and wavelengths below 1350 Å. The discrepancies around 1520 Å are likely related to the strong C₂H₂ absorption feature, and might indicate an underestimation of this species at the two

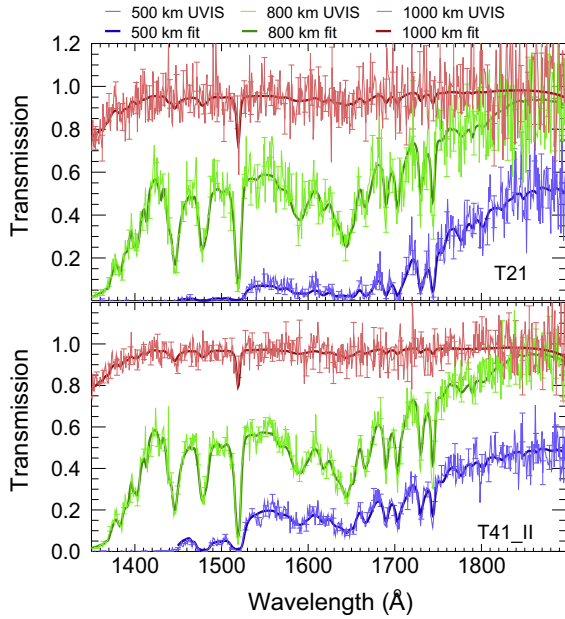


Fig. 5. Measured transmission (light, thin lines) and modeled transmission (dark, thick lines) at 500 km, 800 km, and 1000 km, from flybys T21 and T41_II. Only some uncertainty bars are shown for clarity.

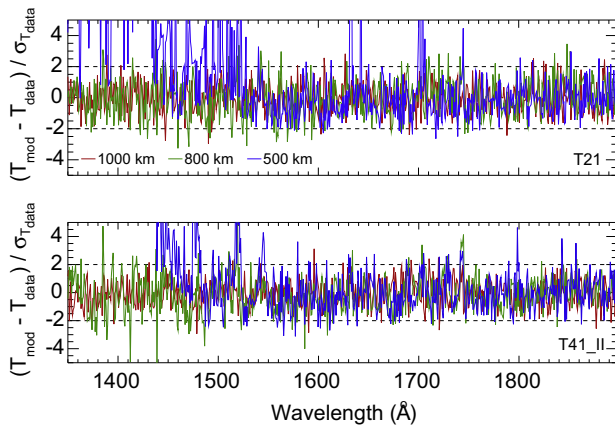


Fig. 6. Normalized transmission residuals for 500 km, 800 km, and 1000 km, from flybys T21 and T41_II. The residuals for T41 and T53 present similar characteristics.

altitudes concerned. A similar comment applies to the discrepancies around 1540 Å, that could indicate a slight underestimation of C_4H_2 . The discrepancies around 1690 and 1700 Å, and those around 1730 and 1740 Å, might indicate a small underestimation of C_2H_4 . Although the benzene signature is not as evident as that of other gasses under visual inspection of the transmission in Fig. 5, its presence is confirmed by the absence of significant residuals in the wavelength region relevant for benzene absorption and by the improvement of the fit statistics when benzene is included. More details about benzene detectability in the UVIS spectra can be found in Koskinen et al. (2011). These authors also observed the discrepancies mentioned above between model transmission and measured transmission. The residuals for T41 and T53 have similar characteristics as those shown in Fig. 6. On the whole, there is no clear sign of significant residuals that might indicate a missing species in the model; the column densities we derived thus give a good representation of the FUV-active species at the different altitudes. The column density profiles of benzene are shown in Fig. 7.

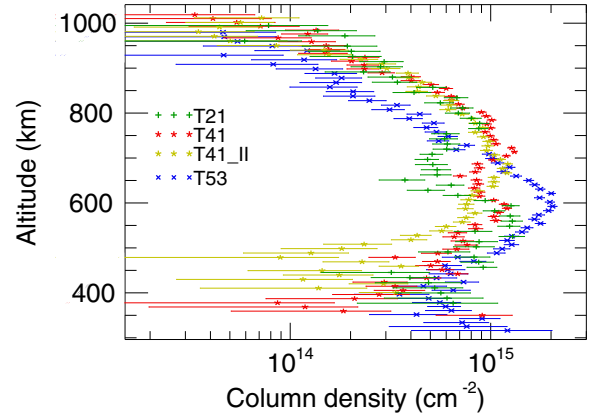


Fig. 7. Benzene column density profiles, for the 4 Stellar occultations analyzed. Horizontal bars show the 1-σ uncertainties.

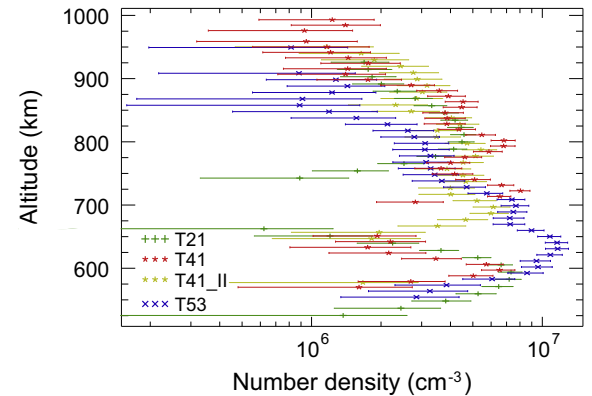


Fig. 8. Benzene number density profiles from the 4 occultations analyzed. Horizontal bars show the 1-σ uncertainties.

5.3. Benzene number densities

We obtained number density profiles for all the species included in the model, and for the 4 occultations. The number density profiles for C_6H_6 in the upper atmosphere of Titan are plotted in Fig. 8. Oscillations of about 15–20% in number density and a few tens of km should be interpreted with caution, as might be due to divergences from the real profile caused by the noise in the column densities, not smoothed by the regularization procedure. The altitude resolution of the number density profiles depends on the width of the averaging kernels (which in turn depends on the amount of regularization or smoothing applied by the retrieval process), and on the effective atmospheric sampling, after altitude averaging (Capalbo et al., 2013). The resolutions are 60 km, 20 km, 20 km, and 25 km for T21, T41, T41_II, and T53, respectively.

Benzene profiles in the upper atmosphere, derived from UVIS observations during flybys T41 and T53 have been presented by Koskinen et al. (2011). In this case, the retrieval was performed with a now outdated version of the room temperature $c-C_6H_6$ absorption cross sections presented here. For most of the altitudes, the values presented here differ from those in Koskinen et al. (2011) in less than twice the uncertainty (or 2σ) in our results. The exception are 2 values (one at 600 km and the other at 800 km), for which the difference is still smaller than 3σ . The use of updated and low temperature benzene absorption cross section is one of the reasons for the small differences observed in the $c-C_6H_6$ (and other species) profiles from the two analyses.

The benzene profiles shown in Fig. 8 agree for some altitudes, but they also present marked differences for some others. Among the most evident, is the much smaller abundances derived from the T53 flyby, above roughly 750 km. This is not the case between roughly 600 and 660 km, where the profile from T53 is bigger than the others by a factor larger than 5. The profile from T53 is the latest of the four presented (April 2009), and is the only one which was measured in the northern hemisphere (39°). The profile from T21 follows the general trend of those from T41 and T41_II above 750 km (although much smoother), and the trend of the profiles from T41 and T53 below 600 km. But the benzene abundance from T21 is much smaller than that in the other flybys between 650 and 750 km. The shape of the curve points to a very low minimum that could not be handled by the inversion routines, leaving a gap of data for some altitudes. The profile from T21 is the first (December 2006), and the most southern of the 4 measured (-39°). A very low minimum, like that in the T21 profile, could also be present between 650 and 700 km in the case of T41. This kind of depletion could lead to the inversion routine failure, responsible of the almost complete lack of values below 650 km for T41_II. These depletion regions are also evident, though much more subtle, in the column densities (see Fig. 7). Finally, the profiles from T41 and from T41_II present more oscillations above 700 km than the profiles from the other occultations. The profile from T41 has maxima at the same time (or separated by about one altitude resolution) that the profile from T41_II has minima. On the other hand, the 2σ envelope of the profiles overlap for most of the altitudes. Moreover, we remind that small oscillations (like the one near 740 km in the profile from T41_II) could be artifacts of the retrieval. The differences we observe between equatorial (T41) and low southern latitude (T41_II) observations are of a factor 2.4 at most, both observations taking place with a few hours difference. It has to be noted that T41 is a night occultation, and the T41_II occultation was measured during the day. So diurnal, and not only latitudinal, variability should be taken into account when interpreting these differences.

The differences between the profiles could be due to geographical and/or temporal variability of benzene in the upper atmosphere. Vuitton et al. (2008) proposed a formation of benzene via $C_6H_7^+$ electron recombination near 900 km, which is the main formation region; and from neutral radical reaction in the stratosphere. Benzene is then rapidly depleted by photolysis, and suffers a rapid decrease below 900 km. The model profiles, however, are calculated for global average conditions. Latitudinal variations of benzene abundances in the stratosphere have been reported by Vinatier et al. (2010), from the analysis of CIRS data measured during northern winter (2005–2007). Vinatier et al. (2015) reported temporal variations in the benzene mixing ratios, from the analysis of CIRS data measured during a longer period (2006–2012), including the northern Spring equinox. However, the measurements derived from CIRS for the stratosphere, where benzene abundances depend strongly on latitude, are not directly comparable with our values for the thermosphere. The few observations presented here prevent an analysis of benzene variability in these upper layers, which is out of the scope of the present paper. Nevertheless, the information presented can set the basis for this kind of studies, in combination with other observations, in future publications.

5.3.1. Effect of variations of absorption cross sections with temperature

To see the effect of the small variations with temperature in the absorption cross section of benzene (see Section 3) in the number density profile, the retrieval was performed with benzene absorption cross sections at room temperature, and the number densities compared with those obtained using low temperature absorption

cross sections. This was done for two test occultations: T41 and T53. The use of absorption cross sections measured at low temperature did not lead to a significant improvement of χ_R^2 , which was expected based on the insignificant variations with temperature observed (Section 3.1). However, the number densities retrieved using the absorption cross section measured at room temperature are slightly lower. This can be explained by the fact that, although the maximum at 1790 Å is bigger for low temperatures, the surrounding continuum is smaller. A relative difference profile was calculated as the difference between the profiles derived with absorption cross sections at different temperatures, divided by the uncertainty. The mean of this relative difference profile is 0.4 (for T41), and 0.3 (for T53). For all altitudes, the relative difference is smaller than 2 (smaller than 1 for T53). So, the effect of the small variations in the absorption cross sections with temperature is negligible for the detection of benzene on Titan with UVIS. Curiously, the profiles of HC_3N and C_2H_4 are sensitive to the variation in the $c-C_6H_6$ absorption cross sections, with variations of up to 2σ for some altitudes (although the mean of the relative differences in the profile is close to zero for these species). This could be due to the overlapping of the C_2H_4 and the $c-C_6H_6$ absorption cross section between 1700 and 1850 Å. In the case of HC_3N , although its identification does not depend on its absorption cross section in this wavelength range, it might be influenced by the change in C_2H_4 . The other species were not significantly affected.

5.3.2. Comparison with models and observations

To compare our results with other measurements and models of benzene abundance in Titan, we converted our number densities into mixing ratios. For this, we used the atmospheric mass density profile measured by the Huygens Atmospheric Structure Instrument (HASI, Fulchignoni et al., 2005), after expressing it as number density, assuming an atmosphere composed of 98.52% of N_2 , and 1.48% of CH_4 (Niemann et al., 2010). The 10% uncertainty in the HASI profile was taken into account to calculate the uncertainty in the mixing ratios. As commented before, UVIS FUV stellar occultations probe a region in the atmosphere below that probed by INMS, and above the region probed by CIRS. A detailed comparison with profiles derived from these instruments is not part of the objectives of this work, and therefore we limit our comparison to some values. Fig. 9 shows our profiles together with measurements by INMS (Cui et al., 2009, shown as Cui09, and Magee et al., 2009, Magee09 in the plot), and CIRS (Vinatier et al., 2015, shown as vinatier15). Magee et al. (2009) derived neutral composition of Titan's upper atmosphere from the analysis of 20 Titan flybys. These took place from October 2004 till May 2008. Cui et al. (2009) studied composition and thermal structure of the upper atmosphere based on the analysis of INMS data from 15 Titan flybys, spanning 2.5 years, from April 2005 till November 2007. The values derived from INMS shown in Fig. 9 correspond to global average mixing ratios of C_6H_6 . These values are more than an order of magnitude smaller than our highest values, which lay only some tens of km below those from INMS. Although photochemical models predict a steep decrease of benzene mixing ratio above a maximum at approximately 950 km (see below), this rate of decrease is still not enough to reconcile INMS measurements with UVIS measurements. Fig. 9 is consistent with Fig. 26 in Koskinen et al. (2011), that also compares benzene mixing ratios derived from INMS and CIRS, with those from UVIS measurements during T41. In addition, we show here 3 other profiles derived from UVIS occultations. Although spatial or temporal variability could be hypothesized to explain the differences between the results from UVIS and those from INMS, the fact that all of the profiles derived from UVIS give larger benzene mole fractions than the INMS data makes this hypothesis unlikely.

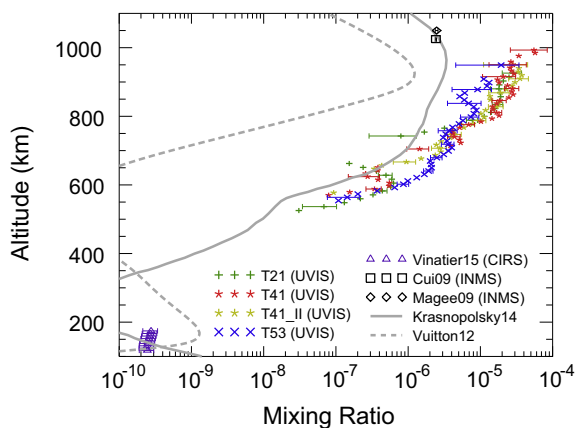


Fig. 9. Benzene mixing ratios derived from stellar occultations measured by UVIS, only some uncertainty bars are shown for clarity. Also shown are profiles from models (Vuitton et al., 2012; Krasnopolsky, 2014), INMS observations (Cui et al., 2009; Magee et al., 2009), and CIRS observations (Vinatier et al., 2015).

The difference between INMS results and UVIS results raises the question of the reliability of the two methods (mass spectrometry and UV spectroscopy). Although INMS results are subject to absolute calibration uncertainties, the instrument measures both N_2 and C_6H_6 , and the ratio should be accurately determined. The density profiles from occultations are more accurate than the INMS densities because they are independent of absolute calibration, but the mixing ratio determination needs to assume an N_2 density profile. We used the HASI density profile (the only profile measured ‘in situ’ reaching the lower altitudes probed by UVIS), which is untypically high when compared to other measurements (see for example Capalbo et al., 2013). Using lower N_2 densities would, however, produce an even larger disagreement between INMS and UVIS. If other species in the atmosphere, non accounted for in our analysis, had extinction characteristics similar to those of benzene in the long wavelength end of the FUV spectrum, the benzene abundance profile derived from the occultations could be overestimated. However, in Section 4.1.3 we presented arguments against this possibility. The difference observed between INMS results and UVIS results should be further explored in the future.

The benzene profile derived from CIRS shown in Fig. 9 (Vinatier et al., 2015) is from the T16 flyby, on July 2006, and corresponds to a latitude of $46^\circ N$, and a longitude of $110^\circ W$. This was chosen because, being the lowest latitude profile in the cited reference, should be closest to the global average. Moreover, it is close in time to the T21 UVIS observation analyzed here. Although the inclusion of the profile derived from CIRS is useful to provide a general picture of benzene abundances, the gap of about 350 km between this profile and those from UVIS, the fact that the values correspond to different times and locations, and the variability of benzene observed in the CIRS data, make it difficult to compare the observations without a more detailed analysis of the behavior of benzene in the stratosphere, out of the scope of the present work (see for example Vinatier et al., 2015).

Fig. 9 also shows benzene profiles from photochemical models: a profile from Vuitton et al. (2012) (from the model called ‘C’ in the paper), shown as Vuitton12, and a profile from Krasnopolsky (2014), shown as Krasnopolsky14. The model in Vuitton et al. (2008) was constrained with INMS and CIRS data, the resulting C_6H_6 mole fraction profiles reproduced well the measurements of these instruments around 1000 km and 100 km, respectively. Vuitton et al. (2012) presented an improved model in which they calculated radiative association reaction rates using transition state theory. They found that, with these changes in the model,

mole fractions can vary by as much as one order of magnitude locally. The dashed gray line in Fig. 9 is a profile from the model in Vuitton et al. (2012). The maximum in the curve at about 923 km is roughly one order of magnitude smaller than the measurements, the difference being more than two orders of magnitude for lower altitudes. The oscillations in the measurements are missed in the model.

Krasnopolsky (2014) compared results from his photochemical model and different observations, for different species, including C_6H_6 . They found that the model reproduces the observational data, within variations comparable to the uncertainty in the measurements and the differences between different measurements. The solid gray line in Fig. 9 represents the C_6H_6 mixing ratio profile in their model. The calculated profile reproduces the general trend of increasing abundance with altitude, but falls short of the values derived from UVIS data by a factor of about 5 in the lowest altitudes, and a factor of about 8 in the highest altitudes. Oscillations in the measured profiles are not reproduced by the model. It is worth mentioning that, in the two models used for the comparison, the profiles are calculated for global average conditions (applicable to low and mid latitudes), solar zenith angle of 60° , and photolysis rates reduced by a factor 2 (to account for the night side). Thus, comparisons with observations at specific time of the day, latitude, and longitude, should be done with caution. Moreover, the large scale oscillations in the measured profiles might be caused by atmospheric waves, not included in the models. Furthermore, the photochemical models are subject to several uncertainties including those in reaction rates. On the whole, although the models reproduce the general trend of mixing ratio increasing with altitude, the data indicate that the models do not produce enough benzene to match the UVIS occultations. Our results imply that the benzene chemistry needs to be re-evaluated.

6. Conclusions

The knowledge of the benzene absorption cross section is mandatory for its detection with UVIS. The absorption cross sections have been thoroughly explored in the past, but an analysis of their temperature dependence was lacking, and presented in this work. We presented absorption cross sections in the range 1153–2103 Å, at 1 Å resolution. This resolution is higher than most the works presented before. We show, for the first time, absorption cross sections in the range 1720–1820 Å for 4 different temperatures in the range 215–298 K. This range is relevant for studies of planetary atmospheres. The measurements are self consistent, and compare well with previous work, apart from some differences in wavelength and cross section value, possibly due to the higher resolution in our measurements. Not much significant variation of the absorption cross sections with temperature was observed, but some temperature effects could be qualitatively and quantitatively analyzed. This variation affects the derivation of benzene profiles on Titan from UVIS data in less than the 1- σ uncertainty in the profiles. However, the cross sections measured at 215 K should be used for the analysis, to avoid a small systematic shift in abundance of the profiles. No further significant variations in the absorption cross section affecting the retrieval with UVIS are expected at lower temperatures. Thus, the spectroscopic data presented in this work are a valuable new addition to the benzene absorption cross section databases. The measurements will become part of a more extensive database of absorption spectra of molecules of astrophysical interest, available online to the scientific community.³

³ Available at <http://www.lisa.u-pec.fr/GPCOS/SCOOPweb/index.html>.

The benzene absorption cross sections measured were added to a larger set of laboratory results, and used to analyze 4 stellar occultations by Titan's atmosphere (T21, T41, T41_II, and T53), observed with the FUV channel of the UVIS instrument. We retrieved column density profiles and number density profiles. Our benzene profiles from T41 and T53, agree well with those in Koskinen et al. (2011), the only previous work that presented this kind of results. They derived benzene profiles from the same occultations, with a similar technique, but an outdated set of absorption cross sections. The four profiles presented here correspond to different times and locations. The differences between each other could, therefore, result from latitudinal or temporal variability of benzene.

The profiles of benzene obtained in the present work cover the altitude gap between the INMS observations and the CIRS observations. Our profiles do not smoothly match globally averaged values derived from INMS. The large difference between INMS values and all 4 UVIS profiles seems unlikely to be explained by temporal or spatial variability. A more thorough comparison should be done to interpret the benzene abundance in the whole altitude range covered by the measurements.

The stellar occultation profiles show a general trend of mixing ratio increasing with altitude, predicted in the profiles from state-of-the-art model calculations. However, in general, the models do not produce enough benzene and fall short of the measurements, and the oscillations in the latter are not reproduced by the former. These differences point to complex chemical and, especially, dynamical processes affecting the benzene vertical distribution, revealed by measurements but not represented by current models. Vertical profiles like the ones derived in this work for benzene, are a fundamental reference to constrain the models, and improve our understanding of Titan's upper atmosphere.

Up to June 2014 we identified 18 stellar occultations measured by UVIS. A preliminary analysis showed that, excluding the four presented here, they present pointing instabilities that make their analysis much more complicated. Although a method has been developed to correct unstable UVIS solar occultations measured with the Extreme Ultraviolet channel (Capalbo, 2014), no such technique has yet been developed for the FUV channel, and remains a challenge for the future. Furthermore, Cassini arrived at the Saturnian system in 2004, and the mission is planned to be continued till 2017. Therefore, some FUV observations during 2 more years are expected to be available. The variability present in current observations could be further examined in the remaining of the Cassini mission, combining observations from different experiments.

Acknowledgments

We are grateful for the valuable help received from the staff at the BESSY II synchrotron facility, during our measurements of benzene absorption. We acknowledge the financial support from the French Space Agency (Centre National d'Études Spatiales, CNES). TTK acknowledges support from the NASA CDAPS Grant NNX14AD51G. We also thank Veronique Vuitton for providing a modeled mixing ratio profile of benzene.

References

- Acton, C.H., 1996. Ancillary data services of NASA's navigation and ancillary information facility. *Planet. Space Sci.* 44 (1), 65–70.
- Ajello, J. et al., 2007. Titan airglow spectra from Cassini ultraviolet imaging spectrograph (UVIS): Euv analysis. *Geophys. Res. Lett.* 34. <http://dx.doi.org/10.1029/2007GL031555> L24204.
- Ajello, J. et al., 2008. Titan airglow spectra from the Cassini ultraviolet imaging spectrograph: Fuv disk analysis. *Geophys. Res. Lett.* 35. <http://dx.doi.org/10.1029/2007GL032315> L06102.
- Bézar, B. et al., 2001. Benzene on the giant planets. *Icarus* 154 (2), 492–500.
- Capalbo, F. et al., 2013. Solar occultation by Titan measured by Cassini/UVIS. *Astrophys. J.* 766 (2), L16. <http://dx.doi.org/10.1088/2041-8205/766/2/L16>.
- Capalbo, F.J., 2014. Titan's Upper Atmosphere Composition and Temperature From Cassini Ultraviolet Imaging Spectrograph Stellar and Solar Occultations, Ph.D. thesis. University of Paris Est.
- Carr, E.P., Stuecklen, H., 1939. An electronic transition of the Rydberg series type in the absorption spectra of hydrocarbons. *J. Chem. Phys.* 7 (8), 631. <http://dx.doi.org/10.1063/1.1750503>.
- Cernicharo, J. et al., 2001. Infrared space observatory's discovery of C₄H₂, C₆H₂, and benzene in CRL 618. *Astrophys. J.* 546 (2), L123–L126.
- Coll, P. et al., 1999. Experimental laboratory simulation of Titan's atmosphere: aerosols and gas phase. *Planet. Space Sci.* 47, 1331–1340.
- Coustenis, A. et al., 2003. Titan's atmosphere from ISO mid-infrared spectroscopy. *Icarus* 161 (2), 383–403.
- Coustenis, A. et al., 2007. The composition of Titan's stratosphere from Cassini/CIRS mid-infrared spectra. *Icarus* 189 (1), 35–62.
- Cui, J. et al., 2009. Analysis of Titan's neutral upper atmosphere from Cassini Ion Neutral Mass Spectrometer measurements. *Icarus* 200 (2), 581–615.
- De La Haye, V. et al., 2008. Coupled ion and neutral rotating model of Titan's upper atmosphere. *Icarus* 197 (1), 110–136.
- Delitsky, M.L., McKay, C.P., 2010. The photochemical products of benzene in Titan's upper atmosphere. *Icarus* 207, 477–484.
- Esposito, L.W. et al., 2004. The Cassini ultraviolet imaging spectrograph investigation. *Space Sci. Rev.* 115, 299–361.
- Fally, S., Carleer, M., Vandaele, A., 2009. Vv fourier transform absorption cross sections of benzene, toluene, meta-, ortho-, and para-xylene. *J. Quant. Spectrosc. Radiat. Transfer* 110 (9), 766–782.
- Feng, R., Cooper, G., Brion, C., 2002. Dipole (e,e⁺ion) spectroscopic studies of benzene: Absolute oscillator strengths for molecular and dissociative photoionization in the VUV and soft X-ray regions. *J. Electron Spectrosc. Related Phenom.* 123 (2), 211–223.
- Ferradaz, T. et al., 2009. Temperature-dependent photoabsorption cross-sections of cyanoacetylene and diacetylene in the mid- and vacuum-UV: Application to Titan's atmosphere. *Planet. Space Sci.* 57, 10–12.
- Fray, N., Schmitt, B., 2009. Sublimation of ices of astrophysical interest: A bibliographic review. *Planet. Space Sci.* 57, 2053–2080. <http://dx.doi.org/10.1016/j.pss.2009.09.011>.
- Fulchignoni, M. et al., 2005. In situ measurements of the physical characteristics of Titan's environment. *Nature*, 438. <http://dx.doi.org/10.1038/nature04314>.
- Grubb, S.G. et al., 1985. Higher excited states of benzene: Symmetry assignments of six gerade Rydberg series by four-photon absorption spectroscopy. *J. Chem. Phys.* 82 (3), 1135. <http://dx.doi.org/10.1063/1.448485>.
- Hammond, V.J. et al., 1950. The absorption spectra of some substituted benzenes and naphthalenes in the vacuum ultra-violet. *Disc. Faraday Soc.* 9, 53–60.
- Hammond, V.J., Price, W.C., 1955. Oscillator strengths of the vacuum ultra-violet absorption bands of benzene and ethylene. *Trans. Faraday Soc.* 51, 605–610.
- Hebrard, E. et al., 2007. Photochemical kinetics uncertainties in modelling Titan's atmosphere: First consequences. *Planet. Space Sci.* 55, 1470–1489.
- Herzberg, G., 1966. Molecular spectra and molecular structure. *Electronic Spectra and Electronic Structure of Polyatomic Molecules*, vol. III. D. Van Nostrand Company Inc.
- Imanaka, H., Smith, M.A., Turro, N.J., 2010. Formation of nitrogenated organic aerosols in the Titan upper atmosphere. *Proc. Nat. Acad. Sci. USA* 107 (28), 12423.
- Khare, B. et al., 1984. Optical constants of organic tholins produced in a simulated titanian atmosphere: From soft X-ray to microwave frequencies. *Icarus* 60 (1), 127–137.
- Koch, E., Otto, A., 1972. Optical absorption of benzene vapour for photon energies from 6 eV to 35 eV. *Chem. Phys. Lett.* 12 (3), 476–480.
- Koch, E., Otto, A., 1976. Vacuum ultra-violet and electron energy loss spectroscopy of gaseous and solid organic compounds. *Int. J. Rad. Phys. Chem.* 8 (1), 113–150.
- Koskinen, T. et al., 2011. The mesosphere and lower thermosphere of Titan revealed by Cassini/UVIS Stellar occultations. *Icarus* 216 (2), 507–534.
- Krasnopolsky, V.A., 2009. A photochemical model of Titan's atmosphere and ionosphere. *Icarus* 201 (1), 226–256.
- Krasnopolsky, V.A., 2014. Chemical composition of Titan's atmosphere and ionosphere: Observations and the photochemical model. *Icarus* 236, 83–91.
- LASP, 2014. Cassini UVIS User's Guide. Laboratory for Atmospheric and Space Physics, Boulder, CO <<http://pds-rings.seti.org/cassini/uvvis/index.html>>.
- Lavvas, P., Coustenis, A., Vardavas, I., 2008. Coupling photochemistry with haze formation in Titan's atmosphere, part ii: Results and validation with Cassini/Huygens data. *Planet. Space Sci.* 56 (1), 67–99.
- Lebonnois, S., 2005. Benzene and aerosol production in Titan and Jupiter's atmospheres: A sensitivity study. *Planet. Space Sci.* 53 (5), 486–497.
- Lebonnois, S., Bakes, E.L.O., McKay, C.P., 2002. Transition from gaseous compounds to aerosols in Titan's atmosphere. *Icarus* 159 (2), 505–517.
- Liang, M.-C., Yung, Y.L., Shemansky, D.E., 2007. Photolytically generated aerosols in the mesosphere and thermosphere of Titan. *Astrophys. J.* 661 (2), L199–L202.
- Magee, B.A. et al., 2009. INMS-derived composition of Titan's upper atmosphere: Analysis methods and model comparison. *Planet. Space Sci.* 57, 1895–1916.
- Markwardt, C.B., 2009. Non-linear least-squares fitting in IDL with MPFIT. In: Bohlender, D.A., Durand, D., Dowler, P. (Eds.), *Astronomical Data Analysis Software and Systems XVIII*, vol. 411. ISBN: 978-1-58381-702-5.
- Niemann, H.B. et al., 2010. Composition of Titan's lower atmosphere and simple surface volatiles as measured by the Cassini-Huygens probe gas chromatograph mass spectrometer experiment. *J. Geophys. Res.: Planets* 115 E12006.

- Pantos, E., Philis, J., Bolovinos, A., 1978. The extinction coefficient of benzene vapor in the region 4.6–36 eV. *J. Mol. Spectrosc.* 72 (1), 36–43.
- Pickett, L.W., Muntz, M., McPherson, E.M., 1951. Vacuum ultraviolet absorption spectra of cyclic compounds. 1. Cyclohexane, cyclohexene, cyclopentane, cyclopentene and benzene. *J. Am. Chem. Soc.* 73 (10), 4862–4865.
- Press, W.H. et al., 1996. Numerical recipes in Fortran 90, . Fortran Numerical Recipes, second ed., vol. 2. Press Syndicate of the University of Cambridge.
- Price, W.C., Walsh, A.D., 1947. The absorption spectra of benzene derivatives in the vacuum ultra-violet. I. *Proc. Roy. Soc. Lond. Ser. A, Math. Phys. Sci.* 191 (1024), 22–31.
- Price, W.C., Wood, R.W., 1935. The far ultraviolet absorption spectra and ionization potentials of C_6H_6 and C_6D_6 . *J. Chem. Phys.* 3 (8), 439.
- Quemerais, E. et al., 2006. Stellar occultations observed by SPICAM on Mars Express. *J. Geophys. Res.* 111. <http://dx.doi.org/10.1029/2005JE002604> E09S04.
- Raulin, F., Toupance, G., Mourey, D., 1982. Organic-syntheses from CH_4-N_2 atmospheres: Implications for Titan. *Origins Life* 12 (3), 267.
- Rennie, E. et al., 1998. A photoabsorption, photodissociation and photoelectron spectroscopy study of C_6H_6 and C_6D_6 . *Chem. Phys.* 229 (1), 107–123.
- Sanchez, R.A., Ferris, J.P., Orgel, L.E., 1966. Cyanoacetylene in prebiotic synthesis. *Science* 154 (3750), 784–785.
- Shemansky, D.E. et al., 2005. The Cassini UVIS stellar probe of the Titan atmosphere. *Science* 308 (5724), 978–982.
- Snowden, D. et al., 2013. The thermal structure of Titan's upper atmosphere, I: Temperature profiles from Cassini INMS observations. *Icarus* 226 (1), 552–582.
- Soderblom, L.A. et al., 2009. Titan from Cassini-Huygens. Springer (Ch. Atmospheric Structure and Composition).
- Suto, M. et al., 1992. Quantitative photoabsorption and fluorescence spectroscopy of benzene, naphthalene, and some derivatives at 106–295 nm. *J. Quant. Spectrosc. Radiat. Trans.* 48 (1), 79–89.
- Turner, D.W., 1970. Molecular Photoelectron Spectroscopy, A Handbook of the 584 Å Spectra. Wiley.
- Vervack, J.R.J., Sandel, B.R., Strobel, D.F., 2004. New perspectives on Titan's upper atmosphere from a reanalysis of the Voyager 1 UVS solar occultations. *Icarus* 170 (1), 91–112.
- Vinatier, S. et al., 2007. Vertical abundance profiles of hydrocarbons in Titan's atmosphere at 15 S and 80 N retrieved from Cassini/CIRS spectra. *Icarus* 188, 120–138.
- Vinatier, S. et al., 2010. Analysis of Cassini/CIRS limb spectra of Titan acquired during the nominal mission. I. Hydrocarbons, nitriles and CO_2 vertical mixing ratio profiles. *Icarus* 205, 559–570.
- Vinatier, S. et al., 2015. Seasonal variations in Titan's middle atmosphere during the northern spring derived from Cassini/CIRS observations. *Icarus* 250, 95–115.
- Vuitton, V. et al., 2006. Experimental and theoretical study of hydrocarbon photochemistry applied to Titan stratosphere. *Icarus* 185 (1), 287–300.
- Vuitton, V. et al., 2012. Rapid association reactions at low pressure: Impact on the formation of hydrocarbons on Titan. *Astrophys. J.* 744 (1), 7pp.
- Vuitton, V., Yelle, R.V., McEwan, M.J., 2007. Ion chemistry and n-containing molecules in Titan's upper atmosphere. *Icarus* 191 (2), 722–742.
- Vuitton, V., Yelle, R.V., Cui, J., 2008. Formation and distribution of benzene on Titan. *J. Geophys. Res.* 113. <http://dx.doi.org/10.1029/2007JE002997> E05007.
- Waite, J.H. et al., 2005. Ion Neutral Mass Spectrometer results from the first flyby of Titan. *Science* 308 (5724), 982–986.
- Wilson, E., Atreya, S., 2003. Chemical sources of haze formation in Titan's atmosphere. *Planet. Space Sci.* 51, 1017–1033.
- Wilson, E.H., Atreya, S.K., 2004. Current state of modeling the photochemistry of Titan's mutually dependent atmosphere and ionosphere. *J. Geophys. Res.* 109 (E6), E06002.
- Wilson, E.H., Atreya, S.K., Coustenis, A., 2003. Mechanisms for the formation of benzene in the atmosphere of Titan. *J. Geophys. Res.* 108 (E2), 8-1–8-10.
- Yoshino, K. et al., 1992. High resolution absorption cross sections in the transmission window region of the Schumann–Runge bands and Herzberg continuum of O_2 . *Planet. Space Sci.* 40 (2), 185–192.